Cu nuclear quadrupole resonance of $YBa_2Cu_3O_x$ with varying oxygen content

Alexander J. Vega, William E. Farneth, Eugene M. McCarron, and Rajendra K. Bordia
Central Research and Development Department, E.I. duPont deNemours and Company, Experimental Station, Building 356, Wilmington, Delaware 19898
(Received 18 August 1988)

^{63}Cu and ^{65}Cu nuclear quadrupole resonance (NQR) results of eleven $YBa_2Cu_3O_x$ samples with x ranging from 7.00 to 6.00 are reported. All measurements were done at room temperature. An attempt was made to quantify integrated signal intensities. The spin-lattice relaxation times (T_1) were either shorter than 0.3 ms or longer than 60 ms. Because the short relaxation times are interpreted as arising from the interaction with conduction electrons, the T_1's could be used to distinguish between metallic and nonconducting substructures. In the $7.0 < x < 6.9$ range where $T_c = 90$ K, the shapes of the NQR spectra were independent of x, but their overall intensity decreased with decreasing oxygen content. In the intermediate range, $6.8 < x < 6.4$ where $T_c = 55$ K, narrow peaks due to nonconducting substructures were observed together with a distinctive short-T_1 line shape, indicating that the (super)conducting state with this oxygen stoichiometry is essentially different from that at $x = 7$. This short-T_1 signal was more pronounced in low-temperature annealed samples for which a T_c of 55 K was observed over a larger x range. It is shown to be consistent with a superordered structure of oxygen vacancies in the conducting substructures. No metallic sites were found for $x < 6.3$ where $T_c \sim 0$. A total of six Cu resonance frequencies were identified between 20 and 32 MHz, some of which could be assigned to specific local crystal structures. In several instances, when the oxygen content was lowered, an NQR peak due to metallic Cu was replaced by a nonmetallic signal at the same frequency. The overall integrated NQR intensity gradually decreased from a value corresponding to three Cu atoms per formula unit for $x = 7$ to 1 Cu for $x = 6$. This is thought to be caused by antiferromagnetic interactions of the electron spins.

I. INTRODUCTION

A number of nuclear quadrupole resonance[1-11] (NQR) and nuclear magnetic resonance[1-3,5,7-10] (NMR) studies of the high-T_c oxide superconductor $YBa_2Cu_3O_x$ have demonstrated that the magnetic resonance properties of the ^{63}Cu and ^{65}Cu nuclei may reveal information pertinent to the understanding of superconductivity in this family of materials. In particular, the temperature dependence of the spin-lattice relaxation times T_1 has been investigated as a tool for characterizing electronic properties of the conducting and superconducting phases.[2,3,5-8] Most of these studies have concentrated on the $YBa_2Cu_3O_x$ stoichiometries which have optimum superconducting properties, i.e., those with x close to 7. A recent exception is the NQR work on $x = 6.7$ and 6.0 compounds by Warren *et al.*[11]

In this paper we report NQR spectra of a series of $YBa_2Cu_3O_x$ samples where the oxygen stoichiometry varies in small steps from $x = 7$ to $x = 6$. Several structural and physical properties have been reported to change dramatically when x is decreased. Particularly interesting is the stoichiometry dependence of the transition temperature T_c.[12-14] The T_c's of samples identical to those used for the present NQR investigation have been previously reported and are plotted vs x in Fig. 1.[13] The figure shows the results obtained for two sets of samples, one (△) prepared by quenching from a high temperature where an equilibrium composition has been reached in an oxygen atmosphere, and the other (●) by reducing high oxygen content samples by low-temperature annealing in vacuum. These results show that T_c gradually decreases from 90 K at $x = 7$ to ~0 K at $x \sim 6.4$, with a plateau around 60 K at $x \sim 6.6$. In addition, conductivity measurements have shown that samples with $x > 6.4$ are metallic above T_c, while the $x < 6.4$ samples are insulators.[14] The magnetic properties are correlated with the conductivity in that the conducting phases are essentially nonmagnetic, whereas compositions in the insulating regime are at least partially antiferromagnetic with Néel temperatures around 400 K.[15-17]

The present magnetic resonance study is intended to provide structural and electronic information at the atomic level which may contribute to the understanding of these phenomena. Our major objective is to characterize structures rather than to examine the mechanism of superconductivity. We are not primarily interested in the superconducting energy gap and, therefore, we restricted our work to room-temperature measurements. We have been careful to make our measurements as quantitative as practically possible. Most of the NQR data were obtained for the samples that were quenched from high temperatures at which oxygen equilibrium was first established. Since T_c is a continuous function of x in this series of samples (see Fig. 1) we may hope that a similarly continuous variation of the NQR spectra will help elucidate the fundamental structural changes that underlie the superconductivity properties. For comparison we have also in-

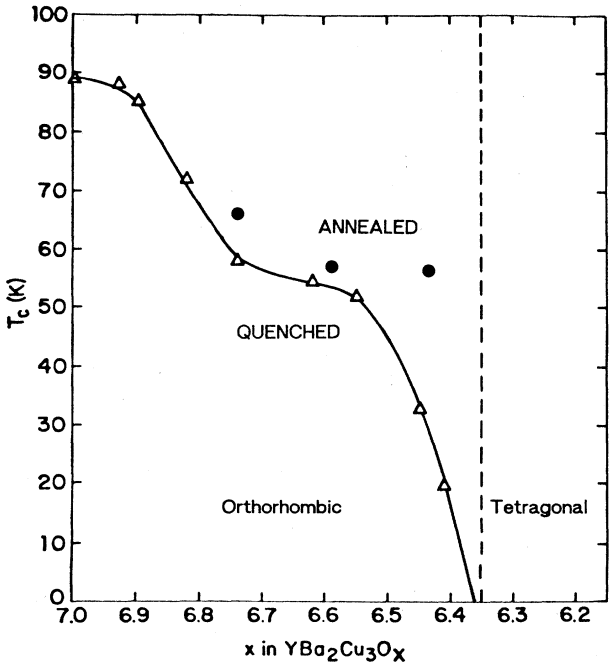

FIG. 1. Onset temperature of magnetic flux exclusion (T_c) vs oxygen stoichiometry for two samples preparation methods of $YBa_2Cu_3O_x$. △ represent quenched from high temperatures; ● represent low-temperature vacuum annealed (from Ref. 13).

vestigated two low-temperature annealed samples which exhibit a better defined T_c plateau for x between 6.4 and 6.6 (Fig. 1).

II. EXPERIMENT

A. Sample preparation

Powders were prepared and oxygen contents established using methods that have been previously described.[13] Briefly, this involves a standard solid-state synthesis of $YBa_2Cu_3O_7$ using binary oxides and BaO_2 as the source of barium. Oxygen contents were fixed by establishing the equilibrium oxygen stoichiometry in air at a given temperature, and rapidly quenching by direct immersion in liquid N_2. Vacuum thermogravimetric analysis (TGA) methods were then used to measure the oxygen stoichiometry of each quenched sample. In each case, the measured stoichiometry was within 0.05 stoichiometry units of that expected from the known equilibrium values at the temperature from which the sample was quenched. The highest oxygen content, $x=7.00$, was attained by additional annealing in oxygen at 350 °C. The starting material for the low-temperature annealed samples was an $x\sim 7$ compound. This material was heated in vacuum at 450 °C in a microbalance assembly. The heating was terminated when the desired weight loss was reached.

A series of similarly prepared samples have been characterized previously by measurements of T_c, Meissner volume fraction, and x-ray powder diffraction. The results of that study have been published elsewhere.[13]

B. Magnetic resonance

The NQR measurements were performed at room temperature with a Bruker CXP300 NMR spectrometer using a probe with a coil insert tunable from 20 to 40 MHz. The rf coil was 3 cm long and its diameter could accommodate 5 mm NMR tubes. The data were obtained with a two-pulse echo sequence,

$$P_{90}-\tau-P_{180}-\tau-\text{detect}, \quad (1)$$

where P_{90} and P_{180} were rf pulses of 4 and 8 μs length, respectively, and τ was 20 μs in all experiments except in T_2 measurements. The NQR line shapes were measured point by point with this echo sequence. The transmitter gain was adjusted to obtain maximum signal intensity of Cu_2O at 26.0 MHz (Refs. 18, 19) and was kept constant over the whole frequency range. At each spectrometer frequency the tuning of transmitter, probe, and receiver preamplifier were optimized. This procedure proved to be adequate for ensuring that P_{90} and P_{180} represented effective "90°" and "180°" pulses over the entire frequency range. Since the effectiveness of rf irradiation is a function of the crystal orientation with respect to the rf-polarization direction,[20] the concepts of 90° and 180° pulses are, at most, loosely defined when powder samples are concerned. One fortunate consequence of this is that the echo intensity as a function of the rf amplitude has a much broader maximum in an NQR echo experiment than in an ordinary NMR spin-echo experiment.

The second half of the echo was detected in quadrature mode with a 0.5 μs dwell time, and was subsequently Fourier transformed. The signal thus obtained represents a slice of the actual NQR line shape, which for the $YBa_2Cu_3O_x$ powders (but not for Cu_2O) is much broader than the spectral area affected by the rf irradiation. Therefore, the signal peaks had a universal shape that was solely determined by the nature of the rf pulses so that relative signal amplitudes could readily be determined by comparison with an arbitrarily chosen reference signal. By comparing complete peak shapes, the intensity determination is not severely affected by random noise and other spurious signals picked up from external radiation sources. Although the width of the Fourier-transformed signals is determined by the rf amplitude, the observed peak is much broader than that because signal components far off resonance are also partially excited. However, we could suppress signal intensity far off resonance by addition of the echoes obtained from (P_{90}, P_{180}) pulses with phases (x,x) and $(-x,y)$ and subtraction of echoes obtained with phases $(-x,x)$ and (x,y). This also eliminated pulse feedthrough signals and baseline artifacts. The line-shape slices obtained in this fashion had a full width at half height of 0.05 MHz.

The measured signal intensities were converted to Cu atom concentrations by dividing by the weight of the Cu contained in the sample and by the square of the resonance frequency. This gave the intensity points that were plotted, in arbitrary units, in the line-shape figures presented in this paper. This numerical procedure is based on the expression for the detected amplitude of

magnetic resonance signals[21]

$$S=f(\nu)NI(I+1)\gamma\nu^2, \quad (2)$$

where ν is the frequency, N is the number of resonating spins, and γ is the gyromagnetic ratio. The function $f(\nu)$ represents the response function of the electronics. In a number of NMR and NQR experiments it was verified that $f(\nu)$ may be considered constant over the frequency range 20–30 MHz, provided the same rf coil is used throughout. In these measurements we compared the NQR signal intensities of ^{35}Cl in K_2IrCl_6 (20.7 MHz) (Ref. 22) and K_2PtCl_6 (25.8 MHz),[23] and of ^{63}Cu and ^{65}Cu in Cu_2O (26.0 and 24.0 MHz).[18,19] Also compared were the ^{35}Cl and ^{37}Cl NMR signal intensities of an aqueous solution of NH_4Cl in a magnetic field of 7.05 T (29.41 and 24.48 MHz). All the results of these measurements agreed well within $\pm 15\%$ with the assumption of a frequency-independent $f(\nu)$ in Eq.(2), while there was no indication of a monotonic change of $f(\nu)$ with increasing ν. Since the error may be as large as $\pm 15\%$, the ratio of the ν's of the two Cu isotopes ($\gamma_{63}/\gamma_{65}=0.933$) may be neglected when the NQR signal intensities of ^{63}Cu and ^{65}Cu (occurring at frequencies with a ratio given by $Q_{63}/Q_{65}=1.083$) are compared. Hence, the intensity ratio is expected to always be equal to the ratio of natural abundances ($n_{63}/n_{65}=2.24$).

One of the major complications in Cu NQR spin counting is T_2 relaxation which reduces the echo intensity by a factor $\exp(-2\tau/T_2)$. For instance, the K_2IrCl_6 signal mentioned above had to be corrected for $T_2=70$ μs, corresponding to a signal reduction to 0.56 when $\tau=20$ μs. Unfortunately, the T_2 decays measured for several $YBa_2Cu_3O_x$ samples at selected frequencies corresponded to signal reductions by factors that range from 0.55 to 0.85. Sometimes the T_2 decays appear to have a Gaussian rather than an exponential τ dependence. In any case, T_2 decay may introduce a spin-count error of $\pm 25\%$. All factors combined, we must conclude that the NQR intensity results reported in this paper may be subject to systematic uncertainties of up to $\pm 40\%$. However, the results obtained for the integrated intensities (see below) suggested that this number is on the pessimistic side.

With the procedure outlined above one may compare quantitative results of different samples and, by comparison with a suitable standard, absolute spin counting should be possible. We have done this with Cu_2O (reduced by heating in argon to convert any CuO to Cu_2O) as a reference. The width of the Cu_2O resonance peak (0.01 MHz), which is much smaller than the spectral "slices" measured by the echo method of Eq.(1), necessitates a method of signal integration that is quite different from the point-by-point addition of the wide $YBa_2Cu_3O_x$ spectra, and thus may cast some doubt on the validity of the intensity comparison. Nevertheless, the integrated intensities of the high- and low-frequency peaks in the $x=7.00$ spectrum determined by this method corresponded to 1.97 and 0.95 Cu atoms per formula unit, respectively (see below). Since we have reason to believe that the $x=7.00$ sample has a nearly ideal vacancy-free crystal structure, and should thus give rise to two signals corresponding to 2 and 1 Cu atom per formula unit, we conclude that the integrated NQR intensities may (with reasonable confidence) be used as a measure of numbers of resonating Cu nuclei.

The actual spectral data points were obtained by signal averaging of between 1000 and 150000 scans with a delay time between scans that ranged from 10 ms to 2 s, depending on the T_1. An exponential multiplication corresponding to a 10 kHz line broadening preceded the Fourier transformation. Spin-lattice relaxation times T_1 were measured with the saturation recovery method. Signal saturation was achieved by application of a sequence of 4 μs x pulses, equally spaced at 20 μs. From the dependence of the signal intensity on the delay time between the saturation and the echo-pulse sequences, T_1 was determined. Because the time scales of the saturation and detection sequences themselves are more than 20 μs, T_1's that were shorter than 100 μs could not be measured accurately. It was often found that the relaxation was characterized by more than one T_1. In those cases, the data were analyzed as a double-exponential decay. When the two T_1's were different by at least two orders of magnitude, we were able to separately measure the line shape of the short-T_1 component by determination of the echo intensities obtained after saturation recovery with an appropriately chosen value of the delay time, usually 1 ms. The NMR data were obtained in a fixed magnetic field of 7.05 T. The frequency dependence of the signal amplitude was measured point by point with an echo method similar to the one described for the NQR experiments. The pulse lengths were 3 and 6 μs; $\tau=10$ μs.

III. RESULTS

A. Line shapes and integrated intensities

The NQR line shapes measured for the series of quenched $YBa_2Cu_3O_x$ samples, with x ranging from 7.00 to 6.09, are shown in Fig. 2. The open symbols in the figure represent intensities of NQR signals having a T_1 relaxation time shorter than 1 ms. In the case of coexisting short- and long-T_1 components, these data points were measured by the presaturation method with a 1 ms recovery time. The filled symbols denote the full signal intensity, i.e., the total of the short-T_1 and long-T_1 components. The spectra in Fig. 2 are normalized to a uniform intensity scale. The integrated signal intensities, converted to Cu atoms per formula unit, are listed in Table I.

The $x=7.00$ line shape agrees with previously published spectra.[1–10] It consists of two ^{63}Cu-^{65}Cu doublets with ^{63}Cu resonance peaks at 22.1 and 31.2 MHz, which have been assigned by others[3,7–11] to the crystallographic Cu(1) sites in the CuO chains and the Cu(2) sites in the CuO_2 planes, respectively (see Fig. 3). When x is decreased from 7 to 6, oxygen atoms are removed from the O(1) positions in the chains.[24–26] This is accompanied by several changes in the intensities, positions, and T_1 characteristics of the peaks shown in Fig. 2. We will attempt to relate these spectral changes to the stoichiometry dependence of the geometric and electronic properties of local Cu environments.

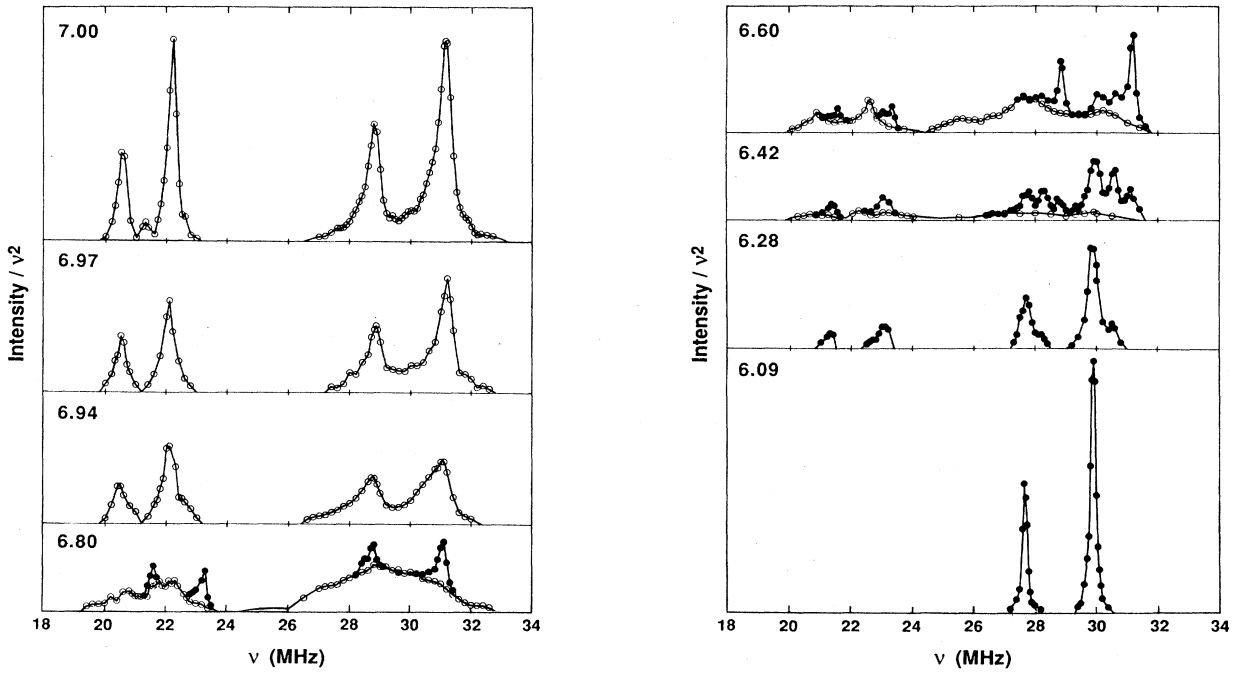

FIG. 2. Cu NQR line shapes of a series of high-temperature quenched $YBa_2Cu_3O_x$ samples for various values of x as indicated. The signal intensities are plotted on a uniform intensity scale, normalized to Cu weight, and divided by the square of the frequency ν. The open symbols represent signal components with $T_1 < 1$ ms. The closed symbols represent signal intensities measured after full T_1-relaxation recovery.

B. Spin-lattice relaxation

Before discussing the line shapes we report the results of T_1 measurements that were carried out for some of the samples at the resonance frequencies of selected line-shape maxima. As stated in Sec. II, the T_1 recoveries were often multiexponential, but in the numerical analysis of the results we assumed the existence of not more than two characteristic relaxation rates. An example is shown in Fig. 4 where the observed signal intensity of the $x=6.80$ sample at 31.2 MHz is plotted versus the delay time which in the T_1 experiment was incremented logarithmically from 50 μs to 3 s. The result of a double-exponential curve fitting is also shown. The plateau around 1 ms clearly demonstrates the coexistence of widely different relaxation rates. The data with delay times shorter than 0.1 ms indicate that the analysis in terms of two exponentials may be an oversimplification, although there is reason to suspect that the measurements at these short times may not be entirely reliable (see Sec. II).

The T_1 results are summarized in Table II. Relaxation times are presented without the relative amplitudes of the

TABLE I. Integrated NQR signal intensities measured in the quenched and annealed (a) $YBa_2Cu_3O_x$ samples. The intensities are converted to numbers of Cu atoms per formula unit.

	20–24 MHz		24–32 MHz		
x	Short T_1	Long T_1	Short T_1	Long T_1	Total
7.00	1.0		2.0		3.0
6.97	0.6		1.3		1.9
6.94	0.6		1.1		1.7
6.80	0.5	0.13	1.4	0.2	2.1
6.60	0.4		1.0	0.4	1.8
6.51(a)	0.2	0.13	0.8	0.5	1.7
6.42	0.2	0.11	0.3	0.6	1.2
6.38(a)	0.13	0.2	0.4	0.7	1.5
6.28		0.14		0.7	0.8
6.09				0.9	0.9
6.00				1.1	1.1

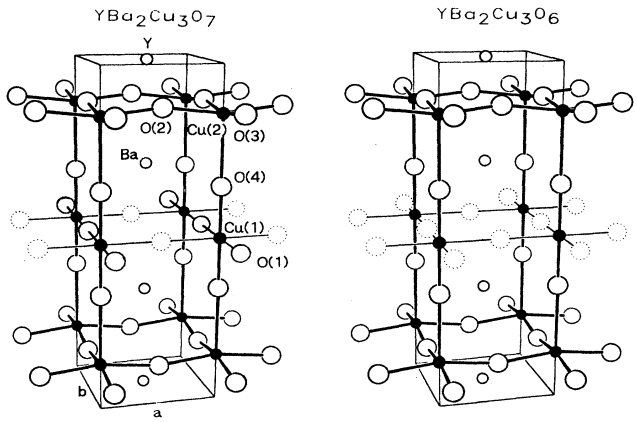

FIG. 3. Crystal structures of $YBa_2Cu_3O_7$ and $YBa_2Cu_3O_6$. Dotted circles indicate oxygen vacancies.

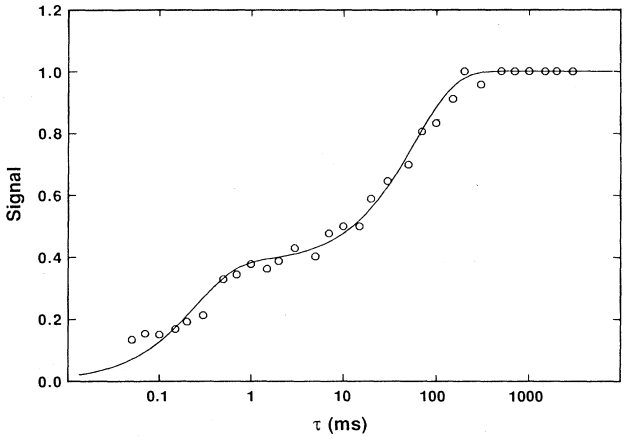

FIG. 4. Signal intensity as a function of the delay time τ, in a saturation recovery experiment at 31.2 MHz of an $YBa_2Cu_3O_{6.80}$ sample, prepared by quenching from a high-temperature oxygen equilibrium. The symbols denote the experimental points. The curve is the result of a fit to a double exponential recovery with $T_1=0.29$ and 62 ms, and respective relative amplitudes of 39% and 61%.

components of double exponentials. The latter are determined by the frequency profiles of the line shapes and for those we refer to Fig. 2 and the following discussion. Table II shows that the T_1's are either shorter than 0.6 ms or longer than 13 ms. In fact, nearly all T_1's fall outside the 0.3–60 ms range, thus forming a bimodal distribution with a gap of two orders of magnitude. Based on the common interpretation of Cu spin-lattice relaxation in conductors and insulators,[2,3,5–9,11] we identify the Cu sites having short T_1 (<1 ms) with structural elements that are conducting, and those having long T_1 (>10 ms) with nonconducting substructures. Thus, the NQR data in Table II show that when x is close to 7.0, all Cu atoms are in conducting environments at room temperature, and when $x<6.4$, no conducting substructures are present. Normal-state resistivity measurements of materials with these oxygen stoichiometries are consistent with this interpretation.[14] In the samples with intermediate stoichiometries of x between 6.8 and 6.4, insulating and conducting substructures coexist.

TABLE II. T_1 relaxation times (in ms) of ^{63}Cu signals measured at room temperature at selected NQR frequencies in several samples of $YBa_2Cu_3O_x$. Double entries indicate double exponential saturation recoveries.

	Frequency (MHz)				
x	22.1	23.0	29.9	30.6	31.2
6.97	0.08				0.3
6.80	0.04/0.4	0.2/25		0.3	0.3/60
6.60	0.04/0.4		0.13/14		0.2/90
6.42		0.6/60	0.07/70	0.07/80	
6.28		30	13/70	100	
6.09			140/800		
6.00			200		

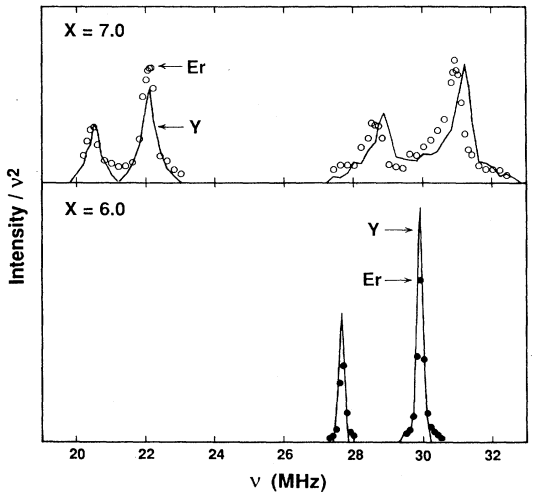

FIG. 5. Cu NQR line shapes of $YBa_2Cu_3O_7$ and $ErBa_2Cu_3O_7$ (top); and $YBa_2Cu_3O_6$ and $ErBa_2Cu_3O_6$ (bottom). The curves and the symbols represent the results measured in the Y and Er samples, respectively. The signal intensities are normalized as in Fig. 2, but the bottom spectra are scaled down by a factor 2 with respect to the top spectra.

C. $x=7.00$

Since the crystal structures of the O_7 and O_6 compositions are best understood, we first discuss the spectra of the highest and lowest x values. As mentioned in Sec. III, the $x=7.00$ line shape agrees with the observation and interpretation of previously published spectra. The integrated intensities of the high- and low-frequency signals (Table I) have the appropriate ratio of 2:1 for the assignment of the 31.2- and 22.1-MHz peaks to coppers in the planes and in the chains, respectively. We note that the 31.2-MHz peak has a shoulder around 30 MHz, which is in fact a spectral region where NQR signals were found in $YBa_2Cu_3O_x$ samples with lower oxygen content (see below).

Further evidence for the peak assignments is obtained from the NQR spectra of $ErBa_2Cu_3O_{7-\delta}$. Er is known to reside exclusively on Y sites.[27] Because of the proximity of this site to the CuO_2 planes (see Fig. 3), the NQR signal of Cu(2) is expected to be affected the most. Figure 5(a) shows that the observed shifts of Er relative to Y are consistent with the above assignment. In addition to a shift of the 31.2-MHz peak to 30.95 MHz, the relaxation times associated with it have also been shorten by the Y-to-Er substitution: T_1 from 0.3 to 0.1 ms and T_2 from 90 to 50 μs. These changes are related to the nuclear relaxation mechanism caused by the unpaired electrons of the paramagnetic Er^{3+} ions. No such changes were found for the 22.1-MHz peak, which remained unchanged in its frequency, as well as in its T_1 (0.07 vs 0.08 ms) and T_2 (90 vs 80 μs).

D. $x=6.00$ and 6.09

The NQR spectra of the x=6.00 and 6.09 stoichiometries have nearly identical line-shape profiles and

slightly different integrated intensities [see Table I and Figs. 2 and 5(b)]. The line shape consists of a single ^{63}Cu-^{65}Cu signal pair at 29.9-27.6 MHz. The integrated intensities are close to 1 Cu per formula unit, suggesting that this is the signal Cu(1). The large jump in resonance frequency from 22.1 MHz ($x=7$) to 29.9 MHz ($x=6$) does not contradict this assignment. On the contrary, the stoichiometry change which is accompanied by a reduction of the chain-Cu coordination from four to two oxygens (see Fig. 3) and by an increase in the number of Cu d electrons, should be expected to have a profound effect on the electric field gradient. Further support for assigning the 29.9-MHz peak to Cu(1) is provided by the NQR spectrum of the Er-substituted $x\sim6$ compound, which is superimposed on the spectrum of the $x=6.00$ Y analog in Fig. 5(b). The Cu peaks in the Y and Er compounds have identical frequencies and widths and comparable integrated intensity and relaxation behavior.

Having identified the Cu(1) signal of the $x=6$ structure, we must now comment on the missing spectral contribution from the planes. In general, we may attribute the absence of NQR signal intensity to one or more of the following causes. (a) The resonance falls outside the investigated frequency range of 20 to 33 MHz. (b) The oxygen vacancies introduce disorder in the local environments of the Cu atoms, spreading the NQR frequencies over such a wide range that the signal is broadened beyond detection. (c) The T_1 relaxation time is excessively long, making the point-by-point signal search so tedious that the signal has been overlooked. (d) The T_2 relaxation time is excessively short, preventing the formation of echoes. Relaxation behavior of this type could be caused by electron spin paramagnetism of the Cu sites. (e) Antiferromagnetic or ferromagnetic ordering of the electron spins shifts the nuclear-magnetic signals beyond the detection range. The least probable possibility may be that of chain-oxygen disorder (b), because if it were effective in obliterating the Cu(2) (plane) signal, it should have an even more profound effect on the Cu(1) spectrum. We have searched for long-T_1 signals (delay times up to 2 s) at several resonance frequencies (22.1, 23.1, 27.0 30.5) to partially ensure that excessively long T_1 is not inhibiting signal detection. On the other hand, since it has been established[15,16] that Cu(1) sites in the $x=6$ structure are nonmagnetic while the Cu atoms in the planes are antiferromagnetically ordered, possibility (e) seems to be the most probable cause for the absence of the Cu(2) signal.

We have also examined the 6.09 sample by NMR in a field of 7.0 T. The NMR spectrum (not shown) represents the $m=\frac{1}{2}\rightarrow\frac{1}{2}$ transition of the Cu(1) nuclei which is broadened to second order by the quadrupole interaction. It has the characteristic line shape of a powder pattern due to an axially symmetric quadrupole tensor with singularities at the high- and low-frequency edges which are shifted from the NMR resonance frequency ν_0 by $-\frac{1}{3}\nu_Q^2/\nu_0$ and $\frac{3}{16}\nu_Q^2/\nu_0$, where ν_Q is the corresponding NQR frequency. The singularities are at 75.9 and 81.75 MHz, which correspond to an NMR frequency of $\nu_0=79.6$ MHz and an NQR frequency of $\nu_Q=29.9$ MHz. This is in excellent agreement with the measured NQR result. We also measured the NMR spectrum of Cu_2O. It showed singularities at 76.81 and 81.31 MHz, which correspond to an NMR frequency of $\nu_0=79.7$. We thus observe a chemical shift of about 0.1 MHz or 1200 ppm for $YBa_2Cu_3O_{6.09}$ with respect to Cu_2O. This is much smaller than the Knight shifts of 1.25% and 0.6% that were found for the $x=7$ compound[9] and is thus in agreement with the nonmetallic character of the $x=6$ samples.

E. $7.00 < x < 6.9$

As may be seen from the first three spectra in Fig. 2, the NQR spectra of samples with small amounts of oxygen vacancies ($x \geq 6.94$) are not very much different from the fully oxidized $x=7$ spectrum. However, the peaks become broader and the overall intensity decreases. This is obviously due to the structural disorder introduced by the oxygen vacancies. Unfortunately, we do not detect a signal of the distorted Cu sites, except for the low-frequency shoulder of the 31.2 MHz-peak which grows in relative intensity when x decreases from 7.00 to 6.94. The measured intensity ratios of the high- and low-frequency signals remains close to 2:1 over this stoichiometry range (see Table I). Thus, the Cu sites in the planes and in the chains are affected to the same extent by the oxygen vacancies in the chains. In Sec. IV we propose a possible model of the vacancies.

F. $6.8 < x < 6.4$

When x is reduced to 6.8 the NQR line shape of the quenched $YBa_2Cu_3O_x$ sample undergoes fundamental changes (Fig. 2). A long-T_1 signal appears and the short-T_1 signals are shifted to different frequency regions. The short-T_1 component, which we assign to the conducting substructures in the crystals, continues to change and to decrease in overall intensity until it completely disappears when x is reduced below 6.4. Its exact line shape is difficult to characterize from the plots in Fig. 2, partly because of the broadening of the individual peaks and the resulting overlap of ^{63}Cu and ^{65}Cu signals. A clearer picture is obtained when the short-T_1 line shapes are separated into the contributions from the two isotopes. Such a numerical deconvolution based on fixed frequency and intensity ratios of the ^{63}Cu and ^{65}Cu signals was carried out. The results are shown in Fig. 6. The temperatures, T_c, of the onset of flux exclusion for each of the samples (from Fig. 1) are indicated next to the line shapes. We notice a strong correlation between the peak positions and T_c. In particular, the T_c plateau region of 55 K (see Fig. 1) is characterized by NQR peaks around 22.5, 27.5, and 30 MHz.

In order to better define the Cu NQR spectrum of the conducting phase in the $T_c\sim55$ K plateau region, we also measured the line shapes of two low-temperature annealed $YBa_2Cu_3O_x$ samples, because these maintain the plateau over a wider range of oxygen stoichiometry and give larger Meissner signals at a given value of x.[13] These spectra are shown in Fig. 7 together with that of the $x=6.42$ quenched sample. The corresponding deconvoluted ^{63}Cu-only, short-T_1-only signals are shown in Fig. 8.

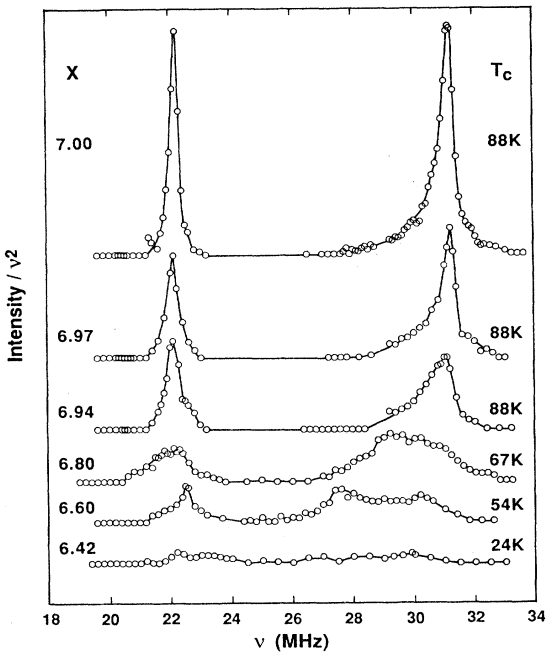

FIG. 6. Short-T_1-only ^{63}Cu-only components of the Cu NQR line shapes of high-temperature quenched $YBa_2Cu_3O_x$ samples with x values as indicated and with T_c values taken from Fig. 1. The plotted data points were obtained by a numerical deconvolution of the short-T_1 components of the spectra shown in Fig. 2. The deconvolution procedure consisted of a least-squares fitting to the sum of two equivalent line shapes, related in frequency by the ratio of the quadrupole moments of ^{63}Cu and ^{65}Cu, and in intensity by the ratio of their natural abundances.

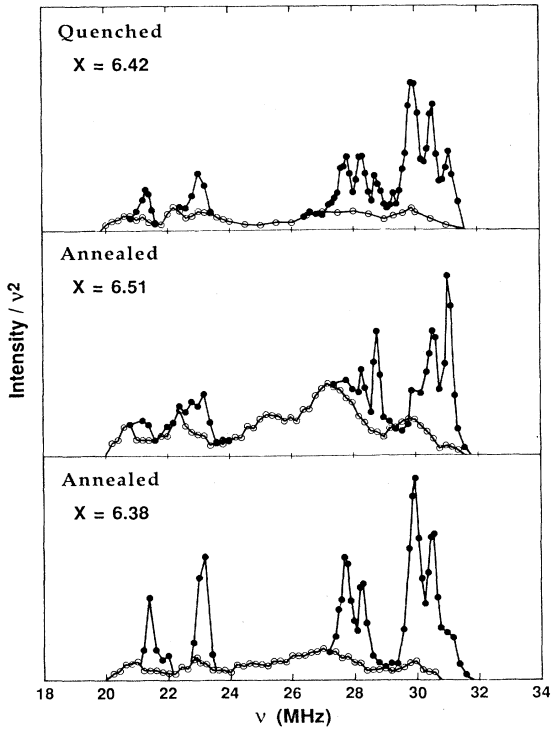

FIG. 7. Cu NQR line shapes of three $YBa_2Cu_3O_x$ samples, one ($x=6.42$) prepared by quenching from a high-temperature oxygen equilibrium, and two ($x=6.51$,6.38) by low-temperature vacuum annealing. Symbols and relative intensities are as in Fig. 2.

Clearly, peaks at 22.5, 27, and 30 MHz are the prominent features of the samples with T_c in the vicinity of 57 K, irrespective of x and thermal history.

Returning to the long-T_1 spectra in Fig. 2, we notice that the signal peaks arising from the insulating portions in the samples are generally sharper than the signals of the conducting structures. This may be interpreted to indicate that the insulating substructures are more uniform in nature than the conducting substructures. The highest x value for which an insulating Cu signal is observed is $x=6.80$. Interestingly its ^{63}Cu peak at 31.2 MHz has the same resonance frequency as Cu(2) in the $x=7.00$–6.94 samples. On the other hand, the long-T_1 signal in the 22-MHz region is shifted to 23.3 MHz.

In the long-T_1 spectra of both the quenched and the annealed samples (Figs. 3 and 6) the intensity of the 31.2-MHz peak gradually diminishes when x decreases to 6.4. Concomitantly, we observe an emerging and steadily growing peak at 29.9 MHz. This peak, which reaches its highest intensity when x approaches 6.0, was already discussed above in connection with the 6.09 and 6.00 spectra and assigned to Cu(1) in the $x=6$ structure. In addition, we see a third high-frequency peak at 30.5 MHz, which is first observed at $x=6.60$, has its highest intensity around $x=6.4$ and gradually becomes weaker at lower oxygen content. Finally, the intensity of the 23-MHz peak remains roughly constant between $x=6.8$ and 6.4.

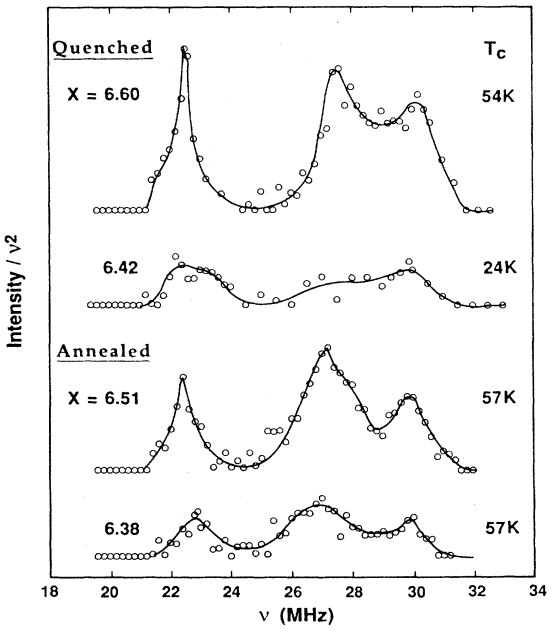

FIG. 8. Short-T_1-only ^{63}Cu-only components of the Cu NQR line shapes of four $YBa_2Cu_3O_x$ samples, two ($x=6.60$ and 6.42) prepared by quenching from a high-temperature oxygen equilibrium, and two ($x=6.51$, 6.38) by low-temperature vacuum annealing. The plotted data points were obtained by a numerical deconvolution of the short-T_1 components of spectra shown in Figs. 2 and 8.

G. $6.3 < x < 6.0$

In the x range where the samples are not superconducting at all ($x < 6.3$), the short-T_1 component is absent in the NQR spectrum. The only observed peaks are the Cu(1) signal at 29.9 MHz and the gradually disappearing signals at 30.5 and 23.1 MHz.

IV. DISCUSSION

There are many characteristics of these data for which we do not have a very clear explanation in terms of the atomic or electronic structure of the material. Therefore, some of what we have to say about the spectra may be naive, and much will be speculative. However, we are confident that linking the NQR data to structural elements of the lattice is an important enterprise that is likely to provide real insight into the electrical and/or magnetic behavior of this material. This confidence comes primarily from the spectra themselves. They are comprised of combinations of a fairly limited number of relatively narrow peaks. The spectral features can be classified into domains of frequency and relaxation times that are widely different and recur through stoichiometry and preparation variations.

The frequencies of the ^{63}Cu peak positions in the NQR spectra of $YBa_2Cu_3O_x$ in Figs. 2 and 6–8 are listed in Table III. They are also summarized in the diagram of Fig. 9, which illustrates the ranges of oxygen stoichiometry over which the various ^{63}Cu peak positions were observed. Short- and long-T_1 signals, arising from conducting and insulating substructures, are indicated by open and cross-hatched bars, respectively. The widths of the bars do not reflect the peak intensities, but rather indicate the frequency range covered by the peaks. In the subsequent discussion we will focus on the narrow features

TABLE III. Peak maxima (in MHz) of ^{63}Cu NQR signals in $YBa_2Cu_3O_x$

x						
			Short T_1			
7.00	22.2					31.15
6.97	22.1					31.2
6.94	22.05					31.05
6.80	~22.0	~22.5		~29	~30.5	
6.60		22.6	27.5	30.1		
6.51		22.4	27.0	29.9		
6.42		22.6		~30.0		
6.38		23.0	27.0	30.0		
			Long T_1			
6.80		23.3				31.05
6.60		23.3		30.1	30.5	31.15
6.51		23.1		30.0	30.6	31.15
6.42		23.0		29.95	30.55	31.1
6.38		23.1		29.95	30.55	
6.28		23.1		29.85	30.5	
6.09				29.90		
6.00				29.90		

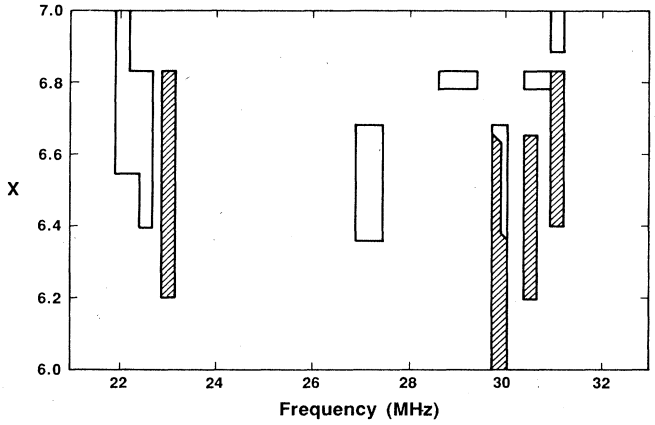

FIG. 9. Schematic summary of ^{63}Cu NQR peak positions in $YBa_2Cu_3O_x$ with x varying from 7 to 6. The open bars denote the x ranges over which short-T_1 signals (due to conducting Cu sites) were observed in Figs. 2, 6, 7, and 8. The cross-hatched bars represent the long-T_1 signals (due to insulating Cu sites).

that extend over wide ranges of x, and ignore the broad features characteristic of transitional regions, i.e., at 26–30 MHz and $x = 6.8$.

It has been shown that the principal changes in the lattice structure as x goes from $6 \rightarrow 7$ in $YBa_2Cu_3O_x$ are associated with the filling of oxygen vacancies on the O(1) site.[24,26] The structures for the limiting stoichiometries O_6 and O_7 are shown in Fig. 3. At intermediate oxygen contents, a variety of local structures are possible including two, three, or four coordination at Cu(1) and four or five coordination at Cu(2). The number of copper atoms that adopt a given coordination depends not only on the total oxygen content, but also on the conditions of preparation for $6 < x < 7$. Therefore, one expects the shapes of the Cu NQR signals, which probe these local structure features to be sensitive to these details as well. Furthermore, associated with each of these atomic framework structures, there is a local electronic structure. It is known from resistivity studies that the superconducting stoichiometries ($x > 6.4$) are metallic at 300 K,[14] while the semiconducting stoichiometries ($x < 6.4$) are antiferromagnetically ordered with a Néel temperature that depends on x.[16] The NQR and NMR data can be particularly useful for probing the relationship between the lattice structure and the electron distribution. Understanding this relationship for the "normal state" is a prerequisite for a detailed description of the superconducting state. The following observations are an attempt to link the spectral features collected in Table III and Fig. 9 with the structural characteristics summarized above.

(1) The NQR spectra show three distinct regimes of electronic structure within the stoichiometry range $O_6 \rightarrow O_7$. The boundaries between these regimes fall at the same stoichiometries as the boundaries between the three types of low-temperature electronic behavior observed with these samples (Fig. 1). At $7.0 > x > 6.9$, all NQR-observable Cu nuclei are in environments that have rapid relaxation rates. Since these are metallic samples,

the rapid relaxation is probably due to metal-like conduction electron dynamics.[2,3,5–9,11] Figure 1 shows that this is also the stoichiometry range of 90 K superconductivity. The clear implication is that the conduction bands must include orbital contributions from both Cu(1) and Cu(2) atoms.

For $6.8 > x > 6.4$ NQR shows a complex mixture of conducting and insulating Cu environments. The detailed NQR peak shapes are a function of both x and preparation conditions within this range. NQR peak shapes are more uniform for the vacuum annealed samples than for the high-temperature quenched materials and seem to preserve the conducting substructures to lower stoichiometries (Fig. 4, 6.38 annealed vs 6.42 quenched). The differences between the quenched and vacuum annealed samples observed by NQR are directly analogous to changes in the T_c vs x curve (Fig. 1) with preparation conditions. Samples prepared by low-temperature vacuum annealing have been shown to extend the $T_c \sim 55$ K phase to lower values of x. Below $x \sim 6.4$ (as noted above, the exact stoichiometry depends on preparation conditions) no Cu atoms are found in conducting environments.[13] These materials are not superconducting.

(2) The integrated signal intensities are reduced when x is decreased from 7.0 to 6.9 (Table I), while the line shape stays essentially unchanged. This indicates that when a small fraction of the O(1) sites is unoccupied (Fig. 3), the numbers of Cu(1) and Cu(2) sites with the atomic and electronic structure of the ideal $x=7$ crystal is reduced. From the initial sharp drop in signal intensity (3.0 for $x=7.00$ to 1.9 for $x=6.97$), we estimate that each oxygen vacancy affects the NQR characteristics of as many as 12 Cu(1) sites and 24 Cu(2) sites. This represents a crystal volume of 12 unit cells around each vacancy, perhaps forming an array extending over four Cu atoms in three adjacent CuO chains. The NQR signals of Cu within the affected areas are not observed, because the local disorder causes them to be spread over a wide frequency range, or because unpaired electrons cause an excessively short T_2. The signal intensity does not continue to decrease linearly with x because areas affected by different vacancies begin to overlap. From the discussion in Sec. II concerning the quantitative aspects of our NQR method, one might conclude that the measured integrated intensities do not warrant quantitative conclusions of this type. We point out, however, that the major intensity errors arise from comparisons between signals at different frequencies. Since we are now comparing signals at the same frequencies and with nearly identical line shapes, most of the errors cancel out.

(3) At several stoichiometries, long-T_1 signals replace short-T_1 signals without a change in resonance frequency. These points are manifested in Fig. 9 by a change from an open bar to a cross-hatched bar at a given frequency. At $x=6.8$, this occurs at 31 MHz, a frequency that at $x=7.0$ has been assigned to Cu(2) (plane) sites. A similar observation was made by Warren *et al.*[11] in an $x=6.7$ compound. Between $x=6.8$ and 6.4 there is a gradual transformation of the short-T_1 signal at 30 MHz to a long-T_1 peak at 29.9 MHz. Finally, between $x=6.8$ and 6.4, the short-T_1 peak around 22.5 MHz gradually gives way to the long-T_1 signal at 23 MHz.

It is remarkable that although oxygen is being removed principally from the coordination sphere of Cu(1), insulating sites appear at $x=6.8$ at frequencies associated with Cu(2). Perhaps, by a perverse coincidence, this frequency (at $x=6.8$) is not the resonance of a Cu(2) nucleus as it is at $x=7.0$, but rather, arises from Cu(1) sites with a lower coordination number than four. However, since the maxima of the short-T_1 signal at $x=7.0$ and the long-T_1 signal at $x=6.8$–6.4 correspond exactly in frequency, we assume that it is five-coordinate Cu(2) site identical to that in the $x=7$ structure. What seems most likely is that removal of oxygen from the coordination sphere of Cu(1) has a direct effect on the electronic structure at some fraction of the Cu(2) sites. This direct effect, involving Cu(1) and Cu(2) atoms closely linked to the new oxygen-vacancy site leads to changes in signal frequencies. Some of the shifted frequencies give rise to the broad short-T_1 component of the spectrum of $x=6.8$ in Fig. 3, while the signals of other directly affected Cu nuclei are not observed at all. On the other hand, there is a subset of Cu(2) nuclei that is unchanged in frequency, but which has a long T_1. This subset must have been created without an appreciable change in the Cu oxidation state or oxygen coordination, although there seems to be a more subtle, indirect effect influencing the relaxation times. We rationalize this as follows. Conduction bands are built up from the progressive interaction of local, single-unit-cell–type electronic wave functions. As long as adjacent "unit-cell structures" are identical, states overlap and eventually broaden into bands. If this progression were stopped at some finite size, by local heterogeneity in the orbital energies, structural domains with discrete rather than continuous-electronic-state density would result. The creation of these isolated "molecular" substructures could give the key NQR features that we observe—a dramatic shift in relaxation times for some fraction of the Cu atoms without an appreciable change in resonance frequency. The boundaries of such domains would occur at the directly affected Cu(2) sites. For example, the bridging O(4) atom moves away from Cu(2) and toward Cu(1) as oxygen is removed from O(1) sites.[14] This implies a rehybridization of the bonding orbitals at Cu(2) and a mismatch between orbital energies at this site and the unperturbed region of the Cu(2) plane. A similar explanation has been proposed for the T_1 increase accompanying a conductivity decrease in some conducting molecular solids.[28]

(4) At $x=6.00$, only Cu(1) sites are observed in NQR. The ^{63}Cu peak at 29.9 MHz can be assigned to the two-coordinate Cu(1) that is created by complete removal of O(1) atoms along the chains. It is known that the material at this stoichiometry is antiferromagnetically ordered.[15–17] The large hyperfine fields that develop at the Cu(2) sites in the antiferromagnetically ordered state are responsible for the disappearance of this signal. Since it seems that the fully developed magnetic ordering below $x=6.4$ can cause signal loss, perhaps the progressive decrease in total signal intensity as x decreases from $7 \rightarrow 6$ (Table I) is also related to magnetic effects at Cu(2). It may be a manifestation of the local ordering into magnet-

ic domains within the superconducting orthorhombic phase. This possibility has been suggested by magnetic-susceptibility measurements.[16]

(5) Hall-coefficient measurements have shown a large drop in the number of carriers at roughly $x=6.8$.[29] NQR seems to reflect this in the appearance of Cu atoms with long relaxation times at this stoichiometry. Because these insulating substructures include both Cu(1) and Cu(2) sites, it is probably not appropriate to think about superconductivity as occuring exclusively in the planes or exclusively in the chains at any stoichiometry.

(6) The 22.1 and 31.2 MHz NQR peaks at $x=7$ were unambiguously assigned to the Cu(1) and Cu(2) sites. Likewise, the 29.9-MHz peak at $x=6$ could be identified with coppers at Cu(1). Unfortunately, we lack sufficient evidence for definite assignments of the remaining peak positions that are summarized in Table III and Fig. 9. One possible approach to a spectral interpretation of these features would be as follows. The above assumption that the long-T_1 peak at 31.1 MHz in the $x=6.8\rightarrow 6.4$ range arises from Cu(2) environment identical to that of $x=7$, immediately suggests two additional peak assignments. First, if the Cu(2) nuclei resonating at 31 MHz change from conducting to nonmetallic around $x=6.8$, the same should be observed for the adjacent sites in the chains. This implies that the long-T_1 peak at 23.3 MHz, which begins to appear around $x=6.8$, could be assigned to Cu(1) sites with fourfold coordination. Second, the gradual shift of NQR intensity around 29.9 MHz from a short-T_1 to a long-T_1 component suggests that we are observing another example of conducting substructures that become nonmetallic when oxygen is removed. Thus, the 30-MHz short-T_1 peak at $x=6.8\rightarrow 6.4$ may be identified with twofold coordinated Cu(1) sites of the type found in the $x=6$ structure. Taking our speculation one step further, we assign the major short-T_1 peak observed around 27 MHz (Which in the intermediate x region accompanies the 30-MHz peak with at least double its intensity) to conducting Cu(2) sites that are associated with the conducting two-coordinated Cu(1). The metallic signals at 27 and 30 MHz are consistently accompanied by a third short-T_1 peak at 22.5 MHz, probably due to four-coordinated Cu(1). This would imply that the (super)conducting state in the $x=6.8\rightarrow 6.4$ range is made up of superordered subunits containing twofold and fourfold coordinated Cu(1), as has been observed for some $x=0.5$ preparations.[30] All these types of local environments seem to contribute to the conduction-band character. However, we reemphasize that this conclusion is not based on firm spectroscopic evidence and that various entirely different interpretation schemes may be proposed.

(7) Many pictures of the electronic structure of this material have suggested that the conduction bands arise largely from interactions between Cu $3d_{x^2-y^2}$ and O $2p$-type atomic orbitals.[31,32] Conduction pathways involving Cu(2), therefore, are two-dimensional in the a/b plane. Conduction bands involving Cu(1) are localized in the b/c plane. Bands constructed in this way are orthogonal and should not mix within a rigid lattice. However, the NQR data suggest that the electronic properties of the Cu(1) and Cu(2) sites are strongly coupled. There are three indications of that coupling. (a) Cu(1) and Cu(2) sites that can be associated with a particular substructure change intensity proportionately. For example, during the loss in total signal intensity from $x=7.0\rightarrow 6.9$, the relative intensities of the Cu(1) and Cu(2) signals is preserved. (b) Cu(1) sites with short-T_1 relaxation times are observed at stoichiometries as low as 6.4 where the continuity of the Cu(1)-O(1) chains along b must be badly disrupted. If electron moments that could influence Cu(1) relaxation were associated only with conductivity in the b/c plane then one might expect Cu(1) sites to be completely insulating at these high oxygen-vacancy concentrations. (c) Conducting Cu(1) sites with resonance frequencies other than 22.2 MHz are apparently observed. These can only result from local structures that are not part of well-developed chains. These data may be consistent with the superordered structure containing alternating four-coordinate and two-coordinate Cu(1) sites along a, that has been observed for some $x=0.5$ preparations[31] and is consistent with the short-T_1 NQR spectrum of intermediate oxygen stoichiometries as discussed above. However, this superordering must not only preserve the conducting-chain structures to lower stoichiometries, but also incorporate conducting two-coordinate Cu(1) sites. Perhaps O(4)-Cu(1)-O(4) units interact through π-type overlap with the conducting bands of the Cu(2) planes. This type of delocalized structure could be present at any degree of O(1) vacancy, and might lead to short-T_1 Cu(1) signals. However, this is highly speculative and is based on the assumption that short T_1 is always associated with conduction-electron density at the resonant nucleus. The relative contributions of localized and delocalized unpaired electrons in these systems needs to be examined in more detail.

ACKNOWLEDGMENTS

The skilled technical assistance of R. O. Balback and W. R. Dolinger is greatly appreciated.

[1]H. Luetgemeier and M. W. Pieper, Solid State Commun. **64**, 267 (1987).

[2]I. Furo, A. Jánossy, L. Mihály, P. Bánki, I. Pócsik, I. Bakonyi, I. Heinmaa, E. Joon, and E. Lippmaa, Phys. Rev. B **36**, 5690 (1987).

[3]M. Mali, D. Brinkman, L. Pauli, J. Roos, and H. Zimmermann, Phys. Lett. A **124**, 112 (1987).

[4]H. Riesemeier, Ch. Grabow, E. W. Scheidt, V. Mueller, and K. Lueders, Solid State Commun. **64**, 309 (1987).

[5]R. E. Walstedt, W. W. Warren, Jr., R. F. Bell, G. F. Brennert, G. P. Espinosa, J. P. Remeika, R. J. Cava, and E. A. Rietman, Phys. Rev. B **36**, 5727 (1987).

[6]W. W. Warren, Jr., R. E. Walstedt, G. F. Brennert, G. P. Espinosa, and J. P. Remeika, Phys. Rev. Lett. **59**, 1860 (1987).

[7]Y. Kitaoka, S. Hiramatsu, T. Kondo, and K. Asayama, J. Phys. Soc. Jpn. **57**, 30 (1988).

[8]Y. Kitaoka, S. Hiramatsu, K. Ishida, T. Kohara, Y. Oda, K. Amaya, and K. Asayama, Physica B (to be published).

[9]C. H. Pennington, D. J. Durand, D. B. Zax, C. P. Slichter, J. P. Rice, and D. M. Ginsberg, Phys. Rev. B **37**, 7944 (1988).
[10]R. E. Walstedt, W. W. Warren, Jr., R. Tycko, R. F. Bell, G. F. Brennert, R. J. Cava, L. Schneemeyer, and J. Waszczak, Phys. Rev. B **38**, 9303 (1988).
[11]W. W. Warren, Jr., R. E. Walstedt, R. F. Bell, G. F. Brennert, R. J. Cava, G. P. Espinosa, and J. P. Remeika, Physica C **153-155**, 79 (1988).
[12]R. J. Cava, B. Batlogg, C. H. Chen, E. A. Rietman, S. M. Zahurak, and D. Weber, Phys. Rev. B **36**, 5719 (1987).
[13]W. E. Farneth, R. K. Bordia, E. M. McCarron III, M. K. Crawford, and R. B. Flippen, Solid State Commun. **66**, 953 (1988).
[14]W. K. Kwok, G. W. Crabtree, A. Umezawa, B. W. Veal, J. D. Jorgensen, S. K. Malik, L. J. Nowicki, A. P. Paulikas, and L. Nunez, Phys. Rev. B **37**, 106 (1988).
[15]J. M. Tranquada, D. E. Cox, W. Kunnmann, H. Moudden, G. Shirane, P. Zolliker, D. Vaknin, S. K. Sinha, M. S. Alvarez, A. J. Jacobson, and D. C. Johnston, Phys. Rev. Lett. **60**, 156 (1988).
[16]J. M. Tranquada, A. H. Moudden, A. I. Goldman, P. Zolliker, D. E. Cox, G. Shirane, S. K. Sinha, D. Vaknin, D. C. Johnston, M. S. Alvarez, and A. J. Jacobsen, Phys. Rev. B **37**, 3738 (1988).
[17]D. C. Johnston, S. K. Sinha, A. J. Jacobson, and J. Newsam, Physica C **153-155**, 572 (1988).
[18]H. W. de Wijn and J. L. deWildt, Phys. Rev. **150**, 200 (1966).
[19]K. R. Jeffrey and R. L. Armstrong, Can. J. Phys. **44**, 2315 (1966).
[20]T. P. Das and E. L. Hahn, *Nuclear Quadrupole Resonance Spectroscopy* (Academic, New York, 1958), Suppl. 1, p. 15.
[21]A. Abragam, *Principles of Nuclear Magnetism* (Clarendon, Oxford, 1961), p. 72.
[22]Ko. Itoh, D. Nakamura, K. Itoh, and M. Kubo, Inorg. Chem. **2**, 690 (1963).
[23]D. Nakamura, Y. Kurita, K. Itoh, and M. Kubo, J. Am. Chem. Soc. **82**, 5783 (1960).
[24]J. D. Jorgensen, M. A. Beno, D. G. Hinks, L. Soderholm, K. J. Volin, R. L. Hitterman, J. D. Grace, I. K. Schuller, C. U. Segre, K. Zhang, and M. S. Kleefish, Phys. Rev. B **36**, 3608 (1987).
[25]T. Siegrist, S. Sunshine, D. W. Murphy, R. J. Cava, and S. M. Zahurak, Phys. Rev. B **35**, 7137 (1987).
[26]C. C. Torardi, E. M. McCarron III, P. E. Bierstedt, A. W. Sleight, and D. E. Cox, Solid State Commun. **64**, 497 (1987).
[27]C. C. Torardi, E. M. McCarron, M. A. Subramanian, H. S. Horowitz, J. B. Michel, A. W. Sleight, and D. E. Cox, in *Chemistry of High Temperature Superconductors,* ACS Symposium Series, No. 351 (American Chemical Society, Washington, DC, 1987), p. 152.
[28]M. Weger, in *Molecular Metals,* edited by W. E. Hatfield (Plenum, New York, 1979), p. 123.
[29]Z. Z. Wang, J. Clayhold, N. P. Ong, J. M. Tarascon, L.H. Greene, and W. R. McKinnon, in *Novel Superconductivity,* edited by S. A. Wolf and V. Kresin (Plenum, New York, 1987), p. 1061.
[30]M. A. Alario-Franco, J. J. Capponi, C. Chaillout, J. Chenavas, and M. Marezio, Mater. Res. Soc. Symp. Proc. **99**, 41 (1988).
[31]M.-H. Whangbo, M. Evain, M. A. Beno, U. Geiser, and J. M. Williams, Inorg. Chem. **26**, 2566 (1987).
[32]Y. Guo, J.-M. Langlois, and W. A. Goddard III, Science **239**, 896 (1988).